J Mater Sci (2009) 44:234–243
DOI 10.1007/s10853-008-3085-0

Relationship between effective ionic radii, structure and electro-mechanical properties of zirconia stabilized with rare earth oxides M_2O_3 (M = Yb, Y, Sm)

M. Hartmanová · E. E. Lomonova · F. Kubel · J. Schneider · V. Buršíková · M. Jergel · V. Navrátil · F. Kundracik

Received: 3 March 2008 / Accepted: 24 October 2008 / Published online: 27 November 2008

Abstract Zirconia stabilized with various concentrations of rare earth oxides of Yb, Sm and Y with different effective ionic radii ratio between the dopant and host cations was studied. In particular, structure, phase composition, compositional range for existence of cubic solid solutions and their phase transformations, stabilization degree of high-temperature phases and the crystal chemistry and type of solid solutions were investigated. These findings were related to the measured material characteristics, namely the electrical conductivity, microhardness and effective elastic modulus, to elucidate various effects important for practical applications, such as an increase of electrical conductivity due to the pyrochlore phase occurrence or an increase of microhardness arising from the effect of dynamic strain ageing.

M. Hartmanová (✉) · M. Jergel
Institute of Physics, Slovak Academy of Sciences,
84511 Bratislava, Slovakia
e-mail: maria.hartmanova@savba.sk

E. E. Lomonova
General Physics Institute, Russian Academy of Sciences,
119991 Moscow, Russia

F. Kubel
Institute for Chemical Technologies and Analytics,
Vienna University of Technology, 1060 Vienna, Austria

J. Schneider
Institute of Crystallography and Mineralogy,
Ludwig-Maximilians University, 80333 Munich, Germany

V. Buršíková
Department of Physical Electronics, Faculty of Sciences,
Masaryk University, 61137 Brno, Czech Republic

V. Navrátil
Department of Physics, Faculty of Education,
Masaryk University, 60300 Brno, Czech Republic

F. Kundracik
Department of Experimental Physics, Faculty of Mathematics,
Physics and Informatics, Comenius University,
84248 Bratislava, Slovakia

Introduction

Zirconias stabilized with rare earth oxides, such as $ZrO_2 + Yb_2O_3$ (YbSZ), $ZrO_2 + Sm_2O_3$ (SmSZ) and $ZrO_2 + Y_2O_3$ (YSZ), are attractive because of high-temperature applications such as the electrolyte materials in the solid oxide fuel cells (SOFCs), the operating temperature of which is usually about 1000 °C. SOFCs have received much recent attention as the next generation of alternative energy sources. In particular, the current efforts are devoted to the reduction of SOFC costs by downsizing fuel cell systems and lowering the operation temperature which also brings long-term durability. One way of lowering the operating temperature is to use an alternative electrolyte, the oxygen ion conductivity of which is higher than that of the usually used yttria-stabilized zirconia (YSZ). However, a high conductivity of the material itself does not assure its potential as an alternative electrolyte for the intermediate temperature solid oxide fuel cells (IT-SOFCs). The material must also fulfil other requirements including the gas-penetration resistance, reactivity, thermal shock resistance, compatibility with the electrode and interconnection materials, etc. The IT-SOFC operates from about 500 °C to 800 °C under the atmospheric or pressurized conditions depending on the specific cell configuration and system design. Besides it, zirconia-based systems are also known to have good mechanical properties, e.g. high hardness needed for planar SOFCs.

As it is known, some physical properties of the systems with the fluorite (F)-type structure, such as electrical conductivity, change with the ratio between effective ionic radii of dopant and host cations, r_d/r_h, as well as with the charge of migrating ions, the doped cation-oxygen vacancy complexes [1–4]. For instance, the systems containing dopants with similar ionic radii in comparison to their respective host cations have the highest conductivities [5–7]. The critical cation radius, which causes neither expansion nor shrinkage of the fluorite structure, should maximize the ionic conductivity [8]. Some information about the effect of the critical cation radius on mechanical properties can be found in [9]. A similar influence of the cation radii was observed also in ternary systems [3, 9].

The purpose of this paper is to study changes of electrical conductivity and some chosen mechanical characteristics of zirconia systems stabilized with the oxides of rare earths (Yb^{3+}, Sm^{3+}) which accompany the changes of their structure and phase composition resulting from the changes of effective ionic radii ratio between the dopant and host cations, r_d/r_h. These materials are promising candidates for the utilization in IT-SOFCs and planar SOFCs instead of zirconia–yttria (YSZ) system.

Experimental

All three systems under study, $ZrO_2 + Yb_2O_3$, $ZrO_2 + Y_2O_3$ and $ZrO_2 + Sm_2O_3$, were prepared by the same method, directional solidification of the melt using direct *rf* melting in a cold container (the skull technique) [10]. Lattice parameters and phase compositions of all three systems were obtained using Rietveld analysis of the powder X-ray diffraction (XRD) data. AC conductivity was measured using a frequency–response analyser. Impedance diagrams were analysed by the method of electrical equivalent circuit. Microhardness and effective elastic modulus were investigated by the classical Vickers indentation method as well as using the depth sensing indentation (DSI) technique with the exception of the $ZrO_2 + Y_2O_3$ system. The details of preparation and measurements of $ZrO_2 + Yb_2O_3$, $ZrO_2 + Y_2O_3$ and $ZrO_2 + Sm_2O_3$ individual systems are described in [11], [12] and [13], respectively.

Results and discussion

Growth of zirconia-based crystals and ionic radii of stabilizing rare earth cations

Phase relations in the $ZrO_2 + M_2O_3$ (M^{3+} = Y, La–Lu) systems depend on their molar composition and dimensions of host Zr^{4+} and dopant M^{3+} cations. The "dimension factor" of rare earth cations as well as the host cation Zr^{4+} is known to be of significant importance. It affects both the region of the existence of the cubic solid solutions and the ordering processes resulting in the compound formation [14–17]. As it was earlier observed, the growth of zirconia crystals stabilized with rare earth oxides of large ionic radii (Pr, Nd and Ce) leads to a significant decrease of the crystal size [18, 19] and also to phase inhomogeneity of the crystals. Difficulties of the growth are associated with a close proximity of temperatures of the phase transformations to melting temperature of the crystals that affects the crystallization processes [18–23].

In the present study, ZrO_2-based crystalline solid solutions stabilized with Sm, Y and Yb oxides have been grown by directional crystallization of the melt at 10 mm/h. In contrast to Pr, Nd and Ce stabilizing oxides, the use of Sm oxide did not lead to the decrease of the crystal sizes over 1–20 mol% concentration range, whereas in the case of Y and Yb oxides this range is even somewhat wider: 1–25 mol%. Concentration ranges of the stabilizing oxides, those which provide the growth of light-transparent cubic solid solution crystals, differ for Sm, Y and Yb oxides: a significant optical dispersion associated with the occurrence of a second phase was observed in zirconia with 7–8 mol% Sm_2O_3 whereas nothing like this was observed when ZrO_2 was stabilized with the same amounts of Y and Yb oxides.

Crystal chemistry and type of solid solution

Structural stability of solid solutions is determined via compositional changes of their cubic lattice parameter. The lattice parameter of the $ZrO_2 + M_2O_3$ systems can be estimated by taking into account the genetic relationship between the structural types (F), (P), and (C) belonging to the space groups *Fm3m*, *Fd3m* and *Ia3*, respectively [24]. As an example, the fluorite (F)-type structure is shown in Fig. 1.

It is known [24] that oxide compounds form a large group of phases with crystal chemical similarity. Phases of different compositions and stoichiometries are built on a common structural principle and can be represented by a generalized chemical formula.

Changes of symmetry, lattice parameters and coordination numbers of cations are observed at the transition from (F)-type to (P)- or (C)-type structures. However, all structural types of this series are related genetically. In particular, the (P)-type structure for solid solutions can be derived from the (F)-type one by ordered substitution of cations $^{VIII}M^{3+}$ for $^{VIII}Zr^{4+}$ and by elimination of anions $^{IV}O^{2-}$. Here, the cationic sublattice retains the most dense cubic packing of F-type, the coordination $^{IV}O^{2-}$ remains

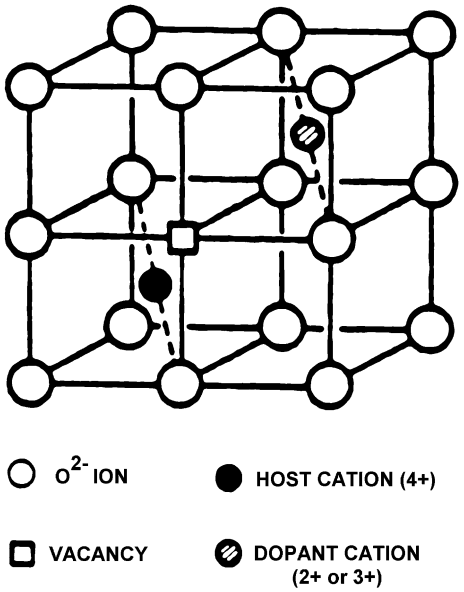

Fig. 1 Structural model of the fluorite-type oxide doped with cations of lower valency; a vacancy occurs in the nearest neighbour position to the dopant cation

and the anionic deficiency leads only to the distortion of oxygen polyhedra [24]. Supposing that there is a direct contact between the cations (Wyckoff position 4a:000) and anions (Wyckoff positions 8c:1/4 1/4 1/4) in the *Fm3m* structure type, one can derive a general formula that describes the influence of the cationic substitutions and the presence of anionic vacancies, V_O^{2-}, on the a_{cal} parameter in the fluorite-like vacant phase of the $(^{VIII}M^{3+})_x$ $(^{VIII}Zr^{4+})_{1-x}(^{IV}O^{2-})_{2-x/2}$ $(V_O^{2-})_{x/2}$ type [24]. In the present study M = Yb, Y and Sm.

The defect reactions associated with the incorporation of M_2O_3 into the zirconia host structure can be written (using Kröger-Vink notation) as follows:

$$M_2O_3 \rightarrow 2M'_{Zr} + V_O^{\bullet\bullet} + 3O_O^x, \quad (1)$$

$$2M_2O_3 \rightarrow 3M'_{Zr} + M_i^{\bullet\bullet\bullet} + 6O_O^x, \quad (2)$$

where M'_{Zr} is a negatively charged substitutional defect and $M_i^{\bullet\bullet\bullet}$ is a positively charged interstitial defect. The Reaction (1) represents the formation of oxygen vacancies $V_O^{\bullet\bullet}$, and Reaction (2) represents the formation of cation interstitials.

The presence of substitutional and interstitial cations M'_{Zr} and $M_i^{\bullet\bullet\bullet}$ as well as anion vacancies $V_O^{\bullet\bullet}$ affects the dependence of the unit cell parameter a_{cal} on the composition and ionic radius r (an interstitial-substitutional mixed solid solution model) according to the relation [24–26]

$$a_{cal} = \frac{4}{(1-y)\sqrt{3}}\left[r\left(M^{3+}, Zr^{4+}\right)_{eff} + (1-y)r\left(O^{2-}\right)_{eff}\right], \quad (3)$$

where effective ionic radius r_{eff} in (4a) position is

$$r\left(M^{3+},\ Zr^{4+}\right)_{eff} = xr\left(^{VIII}M^{3+}\right) + (1-x)r\left(^{VIII}Zr^{4+}\right). \quad (4)$$

The effective anionic radius in (8c) position, $r(O^{2-})_{eff}$, depends on the number of anionic vacancies per one oxygen atom $(1 - x/4)$ and can be written as

$$r\left(O^{2-}\right)_{eff} = r\left(^{IV}O^{2-}\right)\left(1 - \frac{x-2y}{4(1-y)}\right)^{\frac{1}{3}}. \quad (5)$$

The expression $(x - 2y)/4(1 - y)$ represents the vacancy concentration per oxygen atom caused by the cationic substitution diminished by the portion of M^{3+} cations in interstitial positions; $1/(1 - y)$ is the normalization factor and the values of x in the Eqs. 4 and 5 are estimated from the molar composition of systems. The effective ionic radii, r_{eff}, correspond to the incorporated cations (e.g. Yb^{3+}, Y^{3+} and Sm^{3+}) and to the host oxygen anion (O^{2-}). In our case, $r(M^{3+})$ is the cation radius of $r(Yb^{3+}) = 0.0985$ nm, $r(Y^{3+}) = 0.1019$ nm and $r(Sm^{3+}) = 0.1079$ nm; $r(Zr^{4+}) = 0.084$ nm; $r(O^{2-}) = 0.138$ nm [27]. In general, the formation of solid solution $M_xZr_{1-x}O_{2-x/2}$ in the one-phase field proceeds via a substitution of M^{3+} for Zr^{4+} in the special positions of the *Fm3m* space group (Fig. 1). The electroneutrality of substitutional solid solutions ($y = 0$) [24–26] is maintained by the formation of anion vacancies in the oxygen positions. Both lattice parameters, a_{obs} and a_{cal}, are a little different and almost linearly increase with an increase of the dopant amount in all three systems considered in the present study with the exception of the systems with the highest dopant amount used where a slightly steeper increase of a_{obs} is observable (Table 1). Some agreement between the observed and calculated lattice parameters, a_{obs} and a_{cal}, seems to be achievable in the case of higher dopant concentrations introduced into the host zirconia lattice when a smaller or larger part of M^{3+} cations (depending on the ionic radius and amount) enters simultaneously the interstitial positions as it can be concluded from Fig. 2 for the case of Y^{3+} and Sm^{3+}.

For the pure interstitial model ($y = x/4$), the values of a_{cal} deviate significantly from the a_{obs} values for all three systems considered (Table 2). A comparison of the observed (a_{obs}) and calculated (a_{cal}) unit cell parameters confirms the existence of the substitutional (fluorite-type) solid solution $M_xZr_{1-x}O_{2-x/2}$ for all three systems (Figs. 2, 3) with the exception of the solid solutions with the highest M^{3+} cation concentrations (Tables 1, 2).

In the case of mixed-type solid solution, the concentrations of substitutional and interstitial cations as well as the concentration of anion vacancies can be calculated from Eqs. 3–5, putting equality between the observed (a_{obs}) and calculated (a_{cal}) unit cell parameters.

Table 1 Comparison of observed and calculated unit cell parameters, a_{obs} and a_{cal}, for various types of cubic solid solution $M_xZr_{1-x}O_{2-x/2}$ (M = Yb, Y, Sm) according to pure substitutional model, $y = 0$ [24–26] and effective ionic radii [27]

$M_xZr_{1-x}O_{2-x/2}$	r_{eff} (nm)	C (mol% M_2O_3)	a_{obs} (nm)	a_{cal} (nm)
$Yb_{0.200}Zr_{0.800}O_{1.900}$	0.0985	11.10	0.51347	0.51398
$Yb_{0.243}Zr_{0.757}O_{1.879}$		13.80	0.51387	0.51428
$Y_{0.168}Zr_{0.832}O_{1.916}$	0.1019	9.20	0.51453	0.51499
$Y_{0.200}Zr_{0.800}O_{1.900}$		11.10[a]	0.51515[a]	0.51555
$Y_{0.219}Zr_{0.781}O_{1.890}$		12.30	0.51562	0.51583
$Y_{0.243}Zr_{0.757}O_{1.879}$		13.80[a]	0.51599[a]	0.51624
$Y_{0.280}Zr_{0.720}O_{1.860}$		16.30	0.51666	0.51665
$Y_{0.504}Zr_{0.496}O_{1.748}$		33.70	0.52216	0.51948
$Sm_{0.172}Zr_{0.828}O_{1.914}$	0.1079	9.40	0.51663	0.51749
$Sm_{0.182}Zr_{0.818}O_{1.909}$		10.00	0.51771	0.51777
$Sm_{0.200}Zr_{0.800}O_{1.900}$		11.10[a]	0.51749[a]	0.51832
$Sm_{0.243}Zr_{0.757}O_{1.879}$		13.80[a]	0.51812[a]	0.51970
$Sm_{0.244}Zr_{0.756}O_{1.878}$		13.90	0.51787	0.51970
$Sm_{0.314}Zr_{0.686}O_{1.843}$		18.60	0.51949	0.52134
$Sm_{0.601}Zr_{0.399}O_{1.699}$		43.00	1.059	1.05810
				(0.52905)

[a] Values interpolated from the a_{obs} versus C dependences

Table 2 Comparison of observed and calculated unit cell parameters, a_{obs} and a_{calc}, for various types of cubic solid solutions $M_xZr_{1-x}O_{2-x/2}$ (M = Yb, Y, Sm) according to pure interstitial model, $y = x/4$ [25] and effective ionic radii [27]

$M_xZr_{1-x}O_{2-x/2}$	r_{eff} (nm)	C (mol% M_2O_3)	a_{obs} (nm)	a_{cal} (nm)
$Yb_{0.200}Zr_{0.800}O_{1.900}$	0.0985	11.10	0.51347	0.52713
$Yb_{0.243}Zr_{0.757}O_{1.879}$		13.80	0.51387	0.53097
$Y_{0.168}Zr_{0.832}O_{1.916}$	0.1019	9.20	0.51453	0.52543
$Y_{0.200}Zr_{0.800}O_{1.900}$		11.10[a]	0.51515[a]	0.52878
$Y_{0.219}Zr_{0.781}O_{1.890}$		12.30	0.51562	0.53048
$Y_{0.243}Zr_{0.757}O_{1.879}$		13.80[a]	0.51599[a]	0.53306
$Y_{0.280}Zr_{0.720}O_{1.860}$		16.30	0.51666	0.53569
$Y_{0.504}Zr_{0.496}O_{1.748}$		33.70	0.52216	0.55625
$Sm_{0.172}Zr_{0.828}O_{1.914}$	0.1079	9.40	0.51663	0.52872
$Sm_{0.182}Zr_{0.818}O_{1.909}$		10.00	0.51771	0.52971
$Sm_{0.200}Zr_{0.800}O_{1.900}$		11.10[a]	0.51749[a]	0.53170
$Sm_{0.243}Zr_{0.757}O_{1.879}$		13.80[a]	0.51812[a]	0.53676
$Sm_{0.244}Zr_{0.756}O_{1.878}$		13.90	0.51787	0.53676
$Sm_{0.314}Zr_{0.686}O_{1.843}$		18.60	0.51949	0.54301
$Sm_{0.601}Zr_{0.399}O_{1.699}$		43.00	1.059	1.15282
				(0.57641)

[a] Values interpolated from the a_{obs} versus C dependences

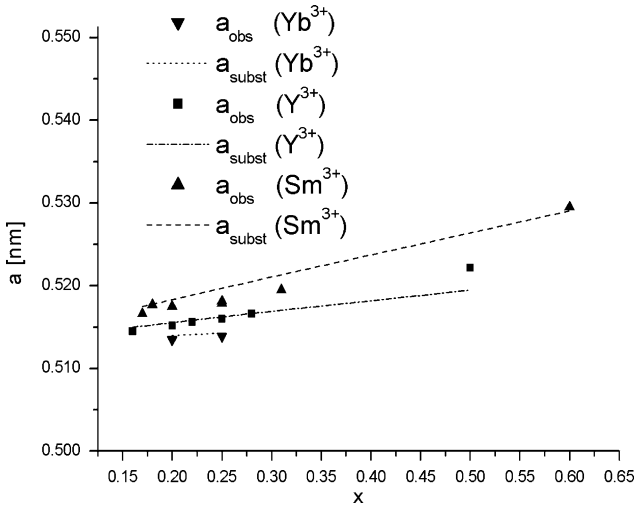

Fig. 2 Observed, a_{obs}, and calculated, a_{subst}, lattice parameters as functions of composition x for the $ZrO_2 + Yb_2O_3$, $ZrO_2 + Y_2O_3$ and $ZrO_2 + Sm_2O_3$ solid solutions (pure substitutional model, $y = 0$)

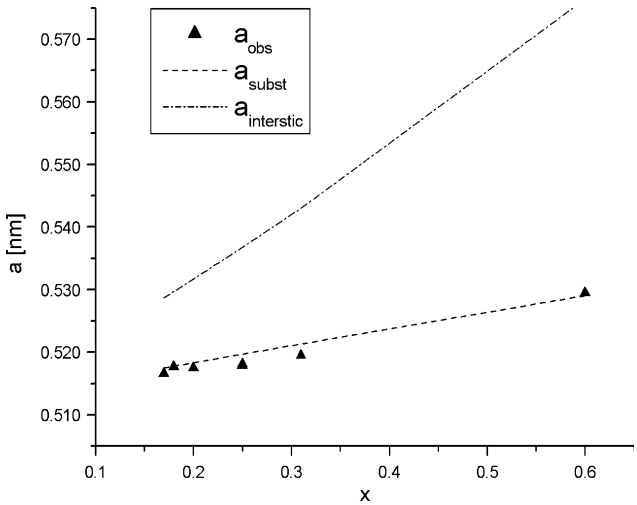

Fig. 3 Observed, a_{obs}, and calculated, a_{subst} and $a_{interstic}$, lattice parameters for pure substitutional ($y = 0$) and interstitial ($y = x/4$) models, respectively, as functions of the composition x for the $ZrO_2 + Sm_2O_3$ solid solutions

In general, all dopant cations (stabilizers) differing in size from the host Zr^{4+} one will distort the host lattice to some extent and influence the migration of oxygen ions through the lattice and thus the electrical conductivity too. The dopants Yb^{3+}, Y^{3+} and Sm^{3+} have different sizes and they are bigger than the host cation Zr^{4+}. Therefore the extent of lattice distortion, in this case the lattice expansion, will be proportional to the size of dopant cation, i.e. the smallest distortion will be in the case of Yb^{3+}, the ionic radius of which is nearest to that of Zr^{4+}. In agreement with that mentioned above and literature data for the (F)-type oxides [28, 29], the unit cell parameters observed, a_{obs}, at our investigations [11–13] increase linearly with increase of the effective ionic radius, r_{eff}, of doping cations Yb^{3+}, Y^{3+} and Sm^{3+} (Figs. 3, 4), and influence the

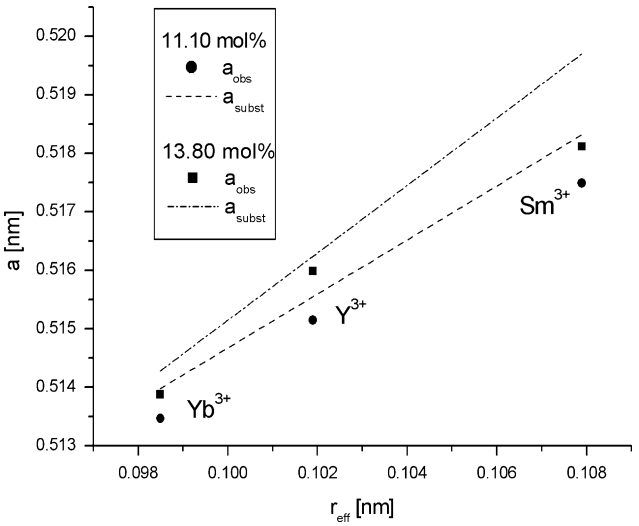

Fig. 4 Observed, a_{obs}, and calculated, a_{subst}, lattice parameters for the pure substitutional model as functions of the effective ionic radius, r_{eff}, for ZrO_2 doped with 11.10 and 13.80 mol% Yb_2O_3, Y_2O_3 and Sm_2O_3

migration of oxygen ions through the lattice and thus the electrical conductivity of the system (see section "Electrical conductivity"). The case of Sc^{3+} cation (e.g. [30]), the ionic radius of which is 0.083 nm and thus very close to that of Zr^{4+}, 0.084 nm is well renown. In this case, the lattice distortion due to different ionic radii of dopant and host cations practically does not exist and electrical conductivity of ZrO_2–Sc_2O_3 system is the highest one among the ZrO_2-based systems. In spite of this fact, this system is not utilized in the SOFCs due to its high cost and problems with ageing [30]. The other situation was found to be in the case of ZrO_2–Sm_2O_3 system, doped with a high amount of samaria, 43 mol%.

As seen from Tables 1, 2 and Figs. 2, 3, the sample with the highest samaria amount of 43 mol%, exhibits the ordered defect fluorite (F)-type structure with the composition $Sm_2Zr_2O_7$ (pure pyrochlore phase) and with the lattice parameter $a_{obs} = 1.059$ nm [13]. This fact is in full agreement with the condition for the ionic radii ratio between dopant and host cations, $r_d/r_h > 1.26$ [1, 15, 28, 29, 31], namely $r(Sm^{3+})/r(Zr^{4+})=1.29$, and for the electron structure [31] to observe the pyrochlore phase. The conditions are not satisfied for the highest yttria amount of 33.70 mol% ($r(Y^{3+})/r(Zr^{4+})=1.21$) where the disordered defect fluorite (F)-type structure with the lattice parameter $a_{obs} = 0.52216$ nm [12] is observed. Similarly, the YbSZ system with $r(Yb^{3+})/(Zr^{4+})=1.17$ does not exhibit the occurrence of the pyrochlore phase [11]. The pure pyrochlore-type structure of the system influences its properties (see sections "Electrical conductivity" and "Mechanical characteristics"). However, as it is possible to find in the literature e.g. Mandal et al. [32–35], an agreement between theoretical modelling reported in the references of this present paper [1, 15, 28, 29, 31] or in [36], according to which some of the materials were predicted to exist in the pyrochlore lattice, and the reality confirmed by a careful XRD, Raman spectroscopic studies, etc. does not exist always. In some cases only a disordered pyrochlore structure, which has a tendency to attain the pyrochlore structure and probably might become a pure pyrochlore under some suitable thermodynamical conditions can be present. Pyrochlore structure of material influences its properties, e.g. electrical conductivity. The structure–electrical conductivity relationship is very important for the materials with fluorite-related structure, including the pyrochlore one, due to the strong dependence of oxygen ion conductivity on the existing phases and their structure (see section "Electrical conductivity").

Electrical conductivity

The electrical conductivity, σ, of all three $ZrO_2 + Yb^{3+}$, $ZrO_2 + Y^{3+}$ and $ZrO_2 + Sm^{3+}$ solid solutions, investigated and discussed together with their corresponding phase compositions in our earlier papers [11–13], has a similar behaviour in terms of its dependence on the structure and phase composition (Fig. 5). As it is shown in our earlier studies [11–13], the highest electrical conductivity was observed for the cubic (c) phase composition in all three investigated systems. It is commonly accepted that a solid solution is formed easily by the addition of a cation with an ionic radius similar to that of the host cation. Among the M^{3+} rare earth cations used in the present study, Yb^{3+} (0.0985 nm) has the nearest radius to that of Zr^{4+} (0.084 nm). The ionic radii of the next two dopants Y^{3+} and Sm^{3+} are larger, being 0.1019 nm and 0.1079 nm, respectively. For all three dopants, the ionic conductivity, σ, decreases as the dopant radius increases. The ionic conductivity of SmSZ is $\approx$60% lower than that of YSZ which itself is $\approx$50% lower than that of YbSZ (inset in Fig. 5). This fact indicates that lattice distortion by the substitution of Yb^{3+} for Zr^{4+} does not affect severely the migration of oxygen ions in contrast to similar substitutions of Y^{3+} and Sm^{3+}. The decreasing lattice distortion with decreasing ionic radius of the M^{3+} cation would imply that the maximum conductivity is shifted to higher defect concentrations. However, such a trend is impeded by the necessity to stabilize the fluorite phase. If ZrO_2 itself has the (F)-type structure, higher conductivities may be observed at lower defect concentrations. Unfortunately, for the comparison of electrical conductivities of the three investigated systems (from the inset of Fig. 5) fully identical concentrations of Yb, Y and Sm dopants (3.30, 3.24 and 4.00 mol%, respectively) were not used. However, it does not change anything on the fact that in the fluorite

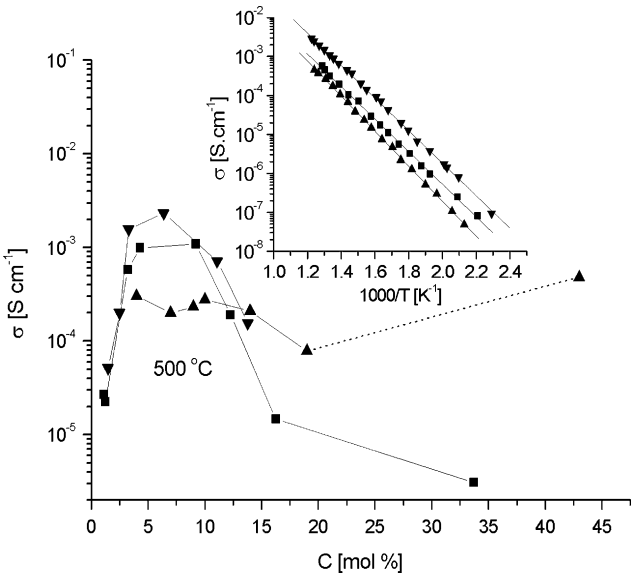

Fig. 5 Electrical conductivity, σ, isotherms as functions of the dopant concentration, C, for the $ZrO_2 + Yb_2O_3$ (▼), $ZrO_2 + Y_2O_3$ (■) and $ZrO_2 + Sm_2O_3$ (▲) solid solutions taken at temperature 500 °C which is interesting as an operating temperature of IT-SOFCs (inset: dependence of electrical conductivity, σ, on the temperature, T, for $ZrO_2 + 3.30$ mol% Yb_2O_3 (▼), $ZrO_2 + 3.24$ mol% Y_2O_3 (■) and $ZrO_2 + 4.00$ mol% Sm_2O_3 (▲) solid solutions)

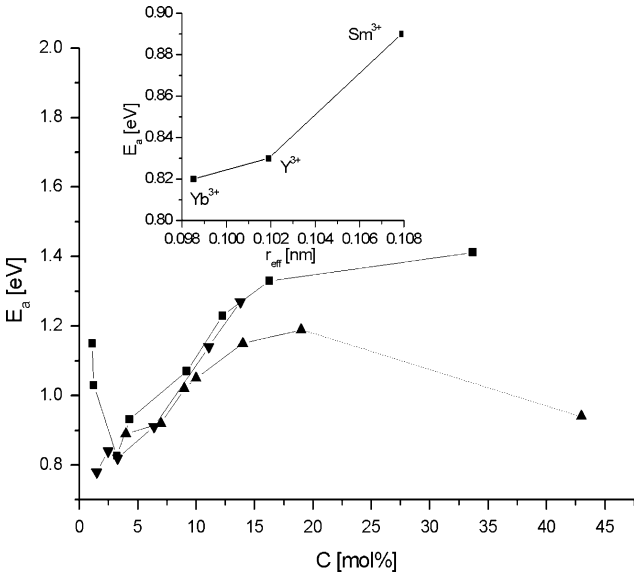

Fig. 6 Activation energy, E_a, as a function of the dopant concentration, C, for the $ZrO_2 + Yb_2O_3$ (▼), $ZrO_2 + Y_2O_3$ (■) and $ZrO_2 + Sm_2O_3$ (▲) solid solutions (inset: dependence of the activation energy, E_a, on the effective ionic radius, r_{eff}, for Yb^{3+}, Y^{3+} and Sm^{3+} doping cations)

phase composition region the electrical conductivity is $\sigma_{Yb} > \sigma_Y > \sigma_{Sm}$ [11–13] and in the pyrochlore phase composition region it is $\sigma_{Yb} < \sigma_Y < \sigma_{Sm}$, which is in full agreement with the literature data of, e.g., Yamamura et al. [1] .

The behaviour and values of the activation energies, E_a, of all three systems are in good agreement with their conductivity behaviour (Fig. 6.), i.e. E_a increases with increasing dopant ionic radius. Enhanced ionic conductivity, σ, observed just for the $ZrO_2 + Yb^{3+}$ system suggests that the lattice distortion and ionic radii ratio play an important role in the electrical conductivity behaviour as follows also from the literature data for these systems (e.g. [5]).

The system with the highest samaria amount of 43 mol% is exceptional among the investigated systems. In general, electrical conductivity of $M_2O_3 + ZrO_2$ systems with higher amounts of M_2O_3 dopant decreases with increasing dopant level due to the decrease of free oxygen vacancy concentration in the anion sublattice of the solid solutions (in our case $M_xZr_{1-x}O_{2-x/2}$). This fact can be explained by increased interactions between the dopant cations and oxygen vacancies resulting in complex defects of low mobility at low temperatures. Similar phenomena explain the conductivity variations in numerous fluorite, perovskite and pyrochlore systems [37]. A deviation from such a conductivity behaviour was observed in the present study just for the largest samaria amount of 43 mol% ($Sm_2Zr_2O_7$) with the pure pyrochlore structure [13]. As it was noticed in section "Crystal chemistry and type of solid solution", electrical conductivity mechanism in a pure pyrochlore is closely connected with its special structure. Pyrochlore structure is a superstructure of defect fluorite structure with exactly twice the lattice parameter [38], in agreement with our studies in [13]. Pure pyrochlore and ideal defect fluorite structures are different because the pyrochlore structure has an additional ordering on both cation and anion sublattices and some of the oxygen ion positions are slightly displaced from their fluorite positions. The oxygen vacancies occur randomly throughout the anion sublattice in the fluorite structure, while being ordered over particular sites (8b) in the pyrochlore structure (see e.g. Fig. 4 in [38]). Structural disorder occurs in the pyrochlore compounds when the superstructure ordering, which is different from the fluorite one, is partially lost. In the (P)-type structure of $Ln_2Zr_2O_7$ due to the special arrangement of Sm^{3+}, Zr^{4+} and O^{2-} ions as well as vacant positions [38], the (P)-type oxides can be intrinsic anion conductors without the dopant-vacancy interactions (e.g. [1, 39]). Disorder of the cation sublattice is relatively less important for the conductivity than that of the anion one, because it has only modest effect on the vacancy mobility. The anions move more easily through the ordered pathways of the pyrochlore structure (cation tetrahedron plane around the 48f oxygen sites) than in the disordered fluorite structure. However, the anion disorder can change the free oxygen vacancy concentration and thus the ionic

conductivity by a few orders of magnitude. In such a way, the observed increased conductivity of ZrO_2 + 43 mol% Sm_2O_3 ($Sm_2Zr_2O_7$) system (Fig. 5) could arise from a reduced oxygen vacancy-dopant cation association stemming from a more open lattice structure due to a special ordering of the cubic phase in agreement with the known influence of pure pyrochlore structure on the electrical conductivity of material (see e. g. papers of Tuller et al. such as [38]). Arrhenius activation energy, E_a, and pre-exponential factor (a measure of the number of mobile ions), σ_0, of materials with the pure pyrochlore structure are smaller than those of other single cubic phase compositions but with lower amounts of Sm_2O_3 due to this special structure of the cubic phase. The concentration behaviour of the activation energy, E_a, and pre-exponential factor, σ_0, of SmSZ is in good agreement with literature data (see e.g. [13]).

Mechanical characteristics

Similar compositional dependences on the effective ionic radii, r_{eff}, as in section "Electrical conductivity", for the three systems under study ZrO_2 + M_2O_3 (M = Yb, Y and Sm), were found also for the microhardness, H, and elastic modulus, Y_{HU}. A gradual lattice distortion with an increasing content of the stabilizing oxides of different ionic radii ($r_{Yb3+} < r_{Y3+} < r_{Sm3+}$) can be seen in the behaviour of both types of microhardness to have been measured (Figs. 7, 8). Vickers microhardness, HV, was measured by the classical quasi-static technique based on the residual indentation caused by plastic deformation:

$$HV = 2\cos 22^\circ \left(L/d^2\right),$$

where L is a load applied on the indenter and d is the indentation diagonal. As an alternative, the plastic microhardness, HU_{pl}, was measured by the DSI technique from the instantaneous depth:

$$HU_{pl} = L_{max}/26.43 \cdot h_r^2,$$

where h_r is the intercept of the unloading curve slope with the indentation depth axis at $L = 0$ and 26.43 is a geometrical factor. Both HV and HU_{pl} increase with increasing amount of M_2O_3 (Yb_2O_3, Y_2O_3 and Sm_2O_3) in the mixed phase composition region, their maximum value being shifted towards higher M_2O_3 amounts in agreement with the increasing effective ionic radius, r_{eff} (Fig. 7—inset). However, the behaviour of microhardness HV as well as HU_{pl} of all three systems is different in the single cubic phase composition region (Fig. 8). In the case of Y_2O_3 dopant, the microhardness of YSZ system is almost independent of the Y_2O_3 amounts used, the data dispersion being attributed to the surface roughness. A significant increase of the microhardness at two largest Yb_2O_3 amounts can be explained by the effect of dynamic strain ageing [40, 41]. In such a case, the diffusion of Yb^{3+} cations to the dislocations and their consequent pinning and hardening of solid solutions are more evident than it is in the case of larger zirconia stabilizers such as Y^{3+} and Sm^{3+} cations where a similar behaviour is expected. The microhardness decrease at the largest Sm_2O_3 amount in the

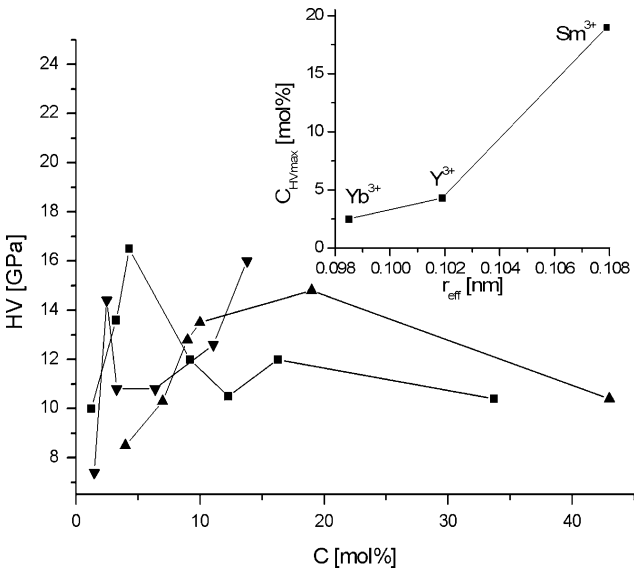

Fig. 7 Vicker's microhardness, HV, as a function of the dopant concentration, C, for the ZrO_2 + Yb_2O_3 (▼), ZrO_2 + Y_2O_3 (■) and ZrO_2 + Sm_2O_3 (▲) solid solutions (inset: shift of the maximum Vickers microhardness, C_{HVmax}, towards higher dopant concentrations depending on the effective ionic radius, r_{eff}, of Yb^{3+}, Y^{3+} and Sm^{3+} doping cations)

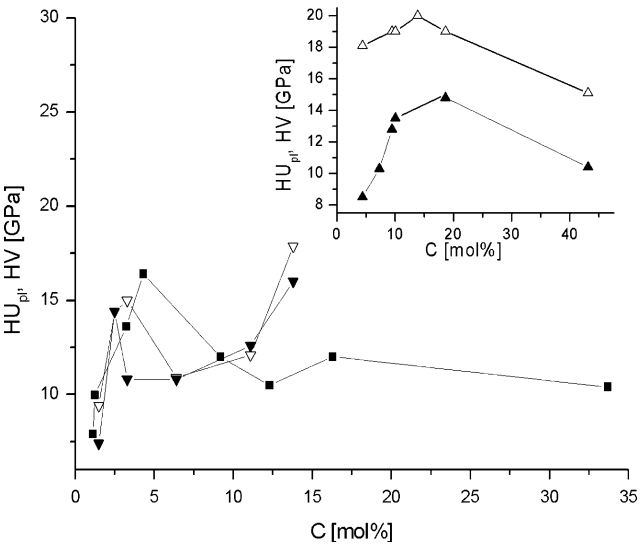

Fig. 8 Comparison of Vickers microhardness, HV, (▼) and plastic microhardness, HU_{pl}, (▽) as functions of the dopant concentration, C, for the ZrO_2 + Yb_2O_3 and Vickers microhardness, HV, (■) for ZrO_2 + Y_2O_3 solid solutions (inset: ZrO_2 + Sm_2O_3 solid solutions, HV (▲) and HU_{pl} (Δ))

pyrochlore phase (Fig. 8—inset) can be ascribed to the special ordering of the cubic structure at the transition from the disordered single cubic (F) to the ordered single cubic (P) phase. The low value of the (P) phase microhardness is in full agreement with the large brittleness of this sample which could be easily destroyed into many small pieces. Generally, the hardening of solid solutions results from an interaction between dislocations and solute atoms, the mechanisms of this interaction being various [42–44].

Mechanical properties, including the elastic modulus, are influenced by the lattice vacancies and lattice parameter. The effect of oxygen vacancy concentration on the elastic modulus, Y_{HU}, of oxides with the fluorite (F)-type structure can be found, for instance, in [45] where it was measured using the nanoindentation test technique at room temperature as in the present study. It is well known that the substitution of a lower valence cation M^{3+} for Zr^{4+} through doping leads to the formation of oxygen vacancies in the lattice. Similarly, the oxygen vacancies are introduced at low oxygen partial pressures, p_{O_2}, into the MO_2 oxides with the fluorite (F)-type structure where charge neutrality is restored by the electrons localized on the host cation to form Ce^{3+} defects in the case of ceria. Another situation can occur in zirconia-based systems such as YSZ. Elastic modulus of YSZ remains unchanged within oxygen partial pressure in the interval $p_{O_2} = 0.21–5 \times 10^{-25}$ atm and temperatures up to 800 °C due to a negligible deviation from the stoichiometry [45]. Experimental results have confirmed the theoretical prediction [46] that the elastic modulus decreases with increasing oxygen vacancy concentration as well as with increase of the lattice parameters due to the defect introduction. The main source of various mechanical effects in materials is due to stresses arising from the lattice-mismatch driven expansion/contraction among the components [47]. The expansion of the lattice due to the presence of defects weakens the attractive forces between the ions. In both cases, the oxygen vacancy and the accompanying presence of lower valent cations result in an average bond length [45] which causes a reduction of the elastic modulus as proposed in [46].

In the present study, the influence of ionic radii ratio, r_d/r_h, between the dopant and host cations of zirconia-based substitutional solid solutions on the elastic modulus is compared. The dopant cations Yb^{3+} and Sm^{3+} have different effective ionic radii r_{eff} and thus different effects on the deformation of the ZrO_2 host lattice. Consequently, the value of lattice parameter (at equal dopant concentrations and equal oxygen vacancy concentrations necessary for charge neutrality) is the main factor controlling the elastic modulus.

The effective elastic modulus, Y_{HU}, was determined from the loading-unloading hysteresis [11, 13], namely from the unloading part of the load-penetration curve:

$$Y_{HU} = \frac{1}{\frac{4\tan(\alpha/2)h_r}{dL/dh(h_{max})\sqrt{\pi}} - \frac{1-\nu_{Dia}^2}{E_{Dia}}},$$

where $Y_{HU} = E/(1 - \nu^2)$ is a so-called indentation modulus or effective elastic modulus (E is the Young's modulus and ν is the Poisson's ratio), $dL/dh(h_{max})$ is the slope of the unloading curve at the maximum indentation depth, h_{max} is the maximum indentation depth at the given maximum load L_{max} and index Dia refers to the indenter material diamond.

The effective elastic modulus Y_{HU} as a function of load L applied on the indenter for ZrO_2 + 13.80 mol% Yb_2O_3 and ZrO_2 + 14.00 mol% Sm_2O_3 with the single cubic phase composition is shown in Fig. 9. It can be seen that the influence of the lattice parameter, a, on the effective elastic modulus, Y_{HU}, is evident mainly at $L > \sim 100$ mN where the measurements are performed at larger depths. This happens in spite of the fact that the indentation in this load region causes the formation of cracks after the unloading period [13], which becomes evident from the decrease of Y_{HU} and from the increase of the data dispersion, in particular for the $ZrO_2 + Sm_2O_3$ system. The value of Y_{HU} for this system is lower than that for $ZrO_2 + Yb_2O_3$ in agreement with the values of the corresponding lattice parameters, $(ZrO_2 + Yb_2O_3) = 0.513877$ nm and $(ZrO_2 + Sm_2O_3) = 0.517873$ nm. The values of Y_{HU} obtained for both systems by the indentation at small depths $L < \sim 100$ mN can be affected by the quality of sample surfaces after their mechanical polishing.

A more complicated situation emerges for both systems in the case of the mixed phase compositions (Fig. 9) where

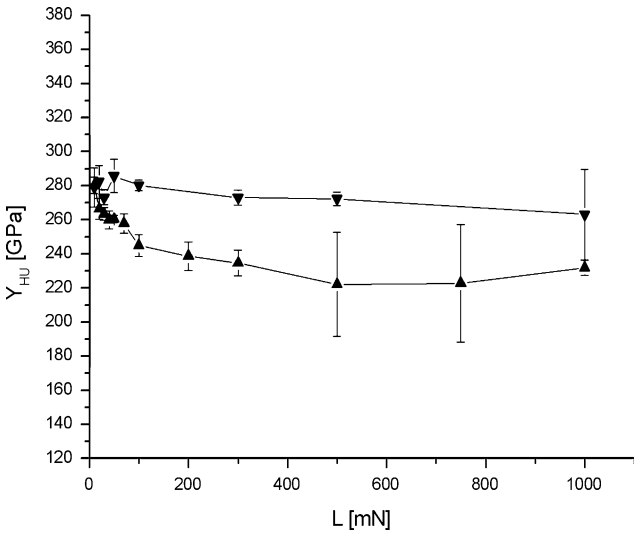

Fig. 9 Effective elastic modulus, Y_{HU}, as a function of the load, L, applied on the indenter for ZrO_2 solid solutions stabilized with 13.80 mol% Yb_2O_3 (▼) and 14.00 mol% Sm_2O_3 (▲)

the values of Y_{HU} obtained at larger depths can be influenced also by fracture formation and phase transformation.

Summary

Structure, phase composition, electrical conductivity, microhardness and effective elastic modulus of zirconia-based solid solutions stabilized by the oxides of rare earths (Yb, Sm, Y) were studied. In particular, their dependence on the effective ionic radii ratio between the dopant and host cations, r_d/r_h, was addressed with the following conclusions:

- stabilization of zirconia-based crystalline solid solutions with rare earth oxides depends on the dimension factor of the dopant rare earth cations, such as Yb^{3+}, Sm^{3+} and Y^{3+}, as well as the host cation Zr^{4+}; width of the compositional window where cubic solid solutions occur and phase transformations close to the crystallization temperature affect crystallization from the melt and phase homogeneity
- besides other factors, the stabilization degree of the zirconia-based high-temperature phases depends strongly on the cationic and anionic radii ratio, r_c/r_a (a possibility to form the cubic fluorite-type structure)
- a stability study in terms of the compositional changes of the lattice parameters of the cubic phases shows:
  - almost all solid solutions under study are substitutional ones with the disordered defect (fluorite-type) structure as concluded from a comparison of the lattice parameters observed, a_{obs}, and calculated, a_{cal}, for the pure substitutional and interstitial models
  - full agreement between the lattice parameters observed, a_{obs}, and calculated, a_{cal}, in the case of higher dopant concentrations could be obtained only when a smaller or larger part of the dopant cations M^{3+} (depending on the ionic radius and amount) enters simultaneously the interstitial positions
  - an unusual value of the lattice parameter was found for the solid solution ZrO_2 + 43 mol% Sm_2O_3 (large dopant amount) with the ordered defect fluorite (F)-type structure and $Sm_2Zr_2O_7$ composition (pure pyrochlore (P) phase), the lattice parameter of which is two times larger than that for the same system with a lower amount of samaria; this fact is in agreement with the condition for the ionic radii ratio to form a pyrochlore (P) phase, $r_d/r_h > 1.26$ ($r(Sm^{3+})/r(Zr^{4+}) = 1.29$)
  - substitution of the dopant cation M^{3+} (e.g. Yb, Y, Sm) for the host cation Zr^{4+} with a smaller effective ionic radius results in the lattice distortion affecting the migration of oxygen ions through the lattice and thus electrical conductivity
- structure and phase composition control the behaviour of the electrical conductivity of all three solid solutions $ZrO_2 + M_2O_3$ (M = Yb, Y, Sm) via the effective ionic radii ratio between the dopant and host cations, r_d/r_h, in particular:
  - electrical conductivity, σ, increases with the decrease of the effective ionic radius r_{eff} of the dopant, i.e. $\sigma(SmSZ) < \sigma(YSZ) < \sigma(YbSZ)$
  - activation energy, E_a, decreases in agreement with the increase of the electrical conductivity, i.e. $E_a(SmSZ) > E_a(YSZ) > E_a(YbSZ)$
  - enhanced electrical conductivity of the solid solution with a large dopant amount ZrO_2 + 43 mol% Sm_2O_3 can be attributed to the single cubic ordered defect fluorite-type structure with the $Sm_2Zr_2O_7$ composition (pure pyrochlore (P)-type structure); the values of the activation energy, E_a, similarly as the pre-exponential factor, σ_0, of this composition are smaller than those of the same systems with smaller dopant amounts and the single cubic disordered defect fluorite-type structure
- values of the Vickers microhardness, HV, plastic microhardness, HU_{pl}, and effective elastic modulus, Y_{HU}, of all three systems are affected by the effective ionic radius, $r_{eff,}$ of the dopant cations M^{3+} ($M^{3+} = Yb^{3+}$, Y^{3+}, Sm^{3+}); in particular:
  - the behaviour of the microhardness (both HV and HU_{pl}) is different in the mixed phase and single cubic compositional regions; in the former region, the microhardness increases with the dopant amount M_2O_3 (M = Yb, Y and Sm) and its maximum value shifts towards larger M_2O_3 amounts in agreement with the increasing effective ionic radius of the dopant cations, $r_{eff;}$ in the latter region, the hardness of YSZ solid solutions is rather independent of the Y_2O_3 amount; a significant enhancement of the microhardness observed in YbSZ can be explained by the effect of dynamic strain ageing. Here, the diffusion of M^{3+} dopant cations to the dislocations and their following pinning as well as the hardening of solid solutions are more distinct than for Y^{3+} and Sm^{3+} dopants with larger effective ionic radii, r_{eff}
  - the decrease of microhardness observed for ZrO_2 + 43 mol% Sm_2O_3 solid solution with the pyrochlore (P)-type structure ($Sm_2Zr_2O_7$) can be attributed to the special ordering of the single cubic structure; the small microhardness value of the

pyrochlore (P) phase is in full agreement with its large brittleness observed

- the effective elastic modulus, Y_{HU}, of the oxide systems with the fluorite-type structure is influenced by the amount of oxygen vacancies and the value of lattice parameter. At equal amount of the oxygen vacancies in $ZrO_2 + Yb_2O_3$ and $ZrO_2 + Sm_2O_3$, the enhanced value of the lattice parameter in the latter system is the main factor reducing its elastic modulus, Y_{HU}.

Acknowledgements The work was partially supported by the research grants No. 2/7119/27 and 2/0047/08 of the Slovak Grant Agency (VEGA), No. 106/05/0274 of the Grant Agency of Czech Republic (GACR).

References

1. Yamamura H, Nishino H, Kakimura K, Nomura K (2003) Solid State Ionics 158:359
2. Taylor MA, Argirusis Chr, Kilo M, Borchardt G, Luther K-D, Assmus W (2004) Solid State Ionics 173:51
3. Kimpton J, Randle TH, Drennan J (2002) Solid State Ionics 149:89
4. Sameshima S, Ono H, Higashi K, Sonoda K, Hirata Y, Ikuma Y (2000) J Ceram Soc Jpn 108:1060 and references herein
5. Strickler DW, Carlsson WG (1965) J Am Ceram Soc 48:286
6. Stattford RJ, Rothman SJ, Routbort JL (1989) Solid State Ionics 37:67
7. Gerhardt-Anderson R, Nowick AS (1981) Solid State Ionics 5:547
8. Kim DJ (1989) J Am Ceram Soc 72:1415
9. Badwal SPS, Ciacchi FT (2000) Ionics 6:1
10. Osiko VV, Lomonova EE, Borik MA (1987) Ann Rev Mater Sci 17:101
11. Hartmanová M, Kubel F, Buršíková V, Navrátil V, Navrátil K, Lomonova EE, Holgado JP, Kundracik F (2008) J Phys Chem Solids 69:805
12. Hartmanová M, Schneider J, Navrátil V, Kundracik F, Schulz H, Lomonova EE (2000) Solid State Ionics 136–137:107
13. Hartmanová M, Kubel F, Buršiková V, Jergel M, Navrátil V, Lomonova EE, Navrátil K, Kundracik F, Kostič I (2007) Russ J Electrochem 43:381
14. Perez-y-Jorba M (1962) Ann Chim (Paris) 7:479
15. Collonques R (1963) Ann Chim (Paris) 8:395
16. Ray SP, Stubican VS (1977) Mater Res Bull 12:549
17. Stubican VS, Hink RC, Ray SP (1978) J Am Ceram Soc 61:18
18. Kuzminov YuS, Lomonova EE, Osiko VV (2004) In: Refractory materials synthetized in cold container. Publishing House NAUKA, Moscow, p 369
19. Aleksandrov VI, Batyugov S Kh, Vishnyakova MA, Voronko Yu K, Kalabukhova VF, Lomonova EE, Osiko VV (1987) Neorg Materiallyi 23:349 (in Russian)
20. Roemer H, Luther K-D, Assmus W (1993) J Cryst Growth 130:233
21. Roemer H, Luther K-D, Assmus W (1994) J Cryst Growth 141:159
22. Roemer H, Luther K-D, Assmus W (1994) Z f Kristallogr 209:314
23. Alisin VV, Borik MA, Lomonova EE, Melshanov AF, Moskvitin GV, Osiko VV, Panov VA, Pavlov VG, Vishnyakova MA (2005) Mater Sci Eng C 25:577
24. Glushkova VB, Hanic F, Sazonova LV (1978) Ceramurgia Int 4:176
25. Hanic F, Hartmanová M, Krcho S (1988) Solid State Ionics 31:167
26. Hartmanová M, Hanic F, Putyera K, Tunega D, Glushkova VB (1993) Mater Chem Phys 34:175
27. Shannon RD (1976) Acta Crystallogr A 32:751
28. Van Dijk MP, De Vries KJ, Burggraaf AJ (1983) Solid State Ionics 9&10:913
29. Hong SJ, Virkar AV (1995) J Am Ceram Soc 78:433
30. Yamamoto O, Arati Y, Takeda Y, Imanishi N, Mizutani Y, Kawai M, Nakamura Y (1995) Solid State Ionics 79:137
31. Pruneda JM, Artacho E (2005) Phys Rev B 72:085107
32. Mandal BP, Garg N, Sharma SM, Tyagi AK (2006) J Solid State Chem 179:1990
33. Mandal BP, Banerji A, Sathe V, Deb SK, Tyagi AK (2007) J Solid State Chem 180:2643
34. Mandal BP, Deshpande SK, Tyagi AK (2008) J Mater Res 23:911
35. Garg N, Pandey KK, Murli Ch, Shanavas KV, Mandal BP, Tyagi AK, Sharma SM (2008) Phys Rev B 77:214105
36. Bevan DJ, Summerville E (1979) In: Gschneider KA Jr, Erying L (eds) Handbook on the physics and chemistry of rare-earths, vol 3. North-Holland, Amsterdam, p 496
37. Kharton VV, Marques FMB, Atkinson A (2004) Solid State Ionics 174:135
38. Tuller HL, Moon PK (1988) Mater Sci Eng B 1:171
39. Minervini L, Grimes RW, Sickafus KE (2000) J Am Ceram Soc 83:1873
40. Van Bueren HG (1960) In: Imperfections in crystals. North-Holland Publishing Company, Amsterdam, p 208
41. Caillard D, Martin JL (2003) In: Thermally activated mechanisms in crystal plasticity. Pergamon, Elsevier, Oxford, p 65
42. Haasen P (1968) Trans Jpn Inst Metals 8(Suppl):40
43. Fleischer RL (1964) In: Strengthening of metals. Einhold Publ., New York
44. Tabor D (2000) In: The hardness of metals. Clarendon Press, Oxford
45. Wang Y, Duncan K, Wachsman ED, Ebrahimi F (2007) Solid State Ionics 178:53
46. Duncan K, Wang Y, Bishop S, Ebrahimi F, Wachsman ED (2006) J Am Ceram Soc 89:3162
47. Yamamoto O (2000) Electrochim Acta 45:2423